JCTC Journal of Chemical Theory and Computation

Article

pubs.acs.org/JCTC

# Another Piece of the Membrane Puzzle: Extending Slipids Further

Joakim P. M. Jämbeck* and Alexander P. Lyubartsev*

Division of Physical Chemistry, Arrhenius Laboratory, Stockholm University, Stockholm, SE-10691, Sweden

Supporting Information

**ABSTRACT:** To be able to model complex biological membranes in a more realistic manner, the force field Slipids (Stockholm lipids) has been extended to include parameters for sphingomyelin (SM), phosphatidylglycerol (PG), phosphatidylserine (PS) lipids, and cholesterol. Since the parametrization scheme was faithful to the scheme used in previous editions of Slipids, all parameters are consistent and fully compatible. The results of careful validation of a number of key structural properties for one and two component lipid bilayers are in excellent agreement with experiments. Potentials of mean force for transferring water across binary mixtures of lipids and cholesterol were also computed in order to compare water permeability rates to experiments. In agreement with experimental and simulation studies, it was found that the permeability and partitioning of water is affected by cholesterol in lipid bilayers made of saturated lipids to the largest extent. With the extensions of Slipids presented here, it is now possible to study complex systems containing many different lipids and proteins in a fully atomistic resolution in the isothermic−isobaric (*NPT*) ensemble, which is the proper ensemble for membrane simulations.

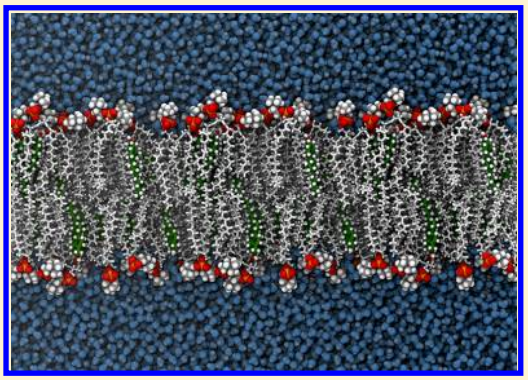

## INTRODUCTION

In both simulation and experimental studies of lipid bilayers, the systems of interest are often composed of one to three components, whereas in biological membranes they contain a vast number of different components.[1−9] Phosphatidylcholines (PC) are the most abundant lipids in mammalian cells,[9] and most studies are performed on these lipids, but other lipids such as phosphatidylethanolamines (PE), sphingomyelins (SM), and cholesterol are also present. For example, SM lipids together with cholesterol are believed to play an important role in the formation of nanodomains in membranes that are often referred to as lipid rafts,[10−12] and a recent study has shown that SM has highly specific interactions with transmembrane domains of proteins.[13] The dynamics of the membrane can be altered by cholesterol since the amount of this stiffening molecule determines the fluidity of the membrane[14] and changes the membrane structure by increasing lipid order, thickness, and bending modulus.[15−21] Different models have been proposed for the area per molecules in binary membrane mixtures, and they all demonstrate cholesterol's condensing effects.[22,23] Furthermore, protein functions can also be regulated by this intriguing molecule.[24−27] X-ray scattering studies suggest that there exist specific interactions between the cholesterol and lipid which are governed by the chemical composition of the lipid molecules and further showed that the mechanical properties of lipid bilayers with different degrees of unsaturation differ when containing cholesterol.[28,29] The amount of cholesterol in cells can also drastically alter the passive diffusion of small molecules through lipid bilayers.[30−32] Other types of lipids, such as ionic ones, e.g., phosphatidylglycerol (PG) and phosphatidylserine (PS), have been documented to interact with membrane bound protein through specific electrostatic interactions[33−35] and are therefore of great importance in biological membranes.

To study the mentioned systems, computer simulations are often used and molecular dynamics (MD) in particular.[36] With MD simulations, it is possible to obtain details on an atomistic resolution, which is difficult to do in experiments due to pronounced thermal fluctuations, the small thickness of the membranes and other reasons. With ever increasing computational power, complex systems like membrane proteins can be simulated on physiologically relevant time scales.[37−39] With accurate models, computer simulations have also been used to predict, e.g., binding free energies of lactoferricin B to membranes.[40,41]

In order for a MD simulation to be accurate, the sampling of phase space has to be sufficient in order to obtain converged results that do not depend on the starting structure. Another crucial element is the applied model Hamiltonian, with the potential energy function called force field (FF). For MD simulations to be able to be used as predictive tools, these two issues have to be dealt with. Lipid bilayers have a history of being difficult systems to simulate in an all-atomistic resolution,[4,42−47] and often a constant surface tension needs to be applied or the membrane area has to be kept constant in order to keep the bilayer from entering the ordered gel phase ($L_{\beta'}$ or $L_{\beta}$). This is however not optimal due to two reasons: (1) deciding on the correct experimental surface area is far from unambiguous,[6] and (2) the proper ensemble for membrane

**Received:** September 7, 2012
**Published:** October 19, 2012

  

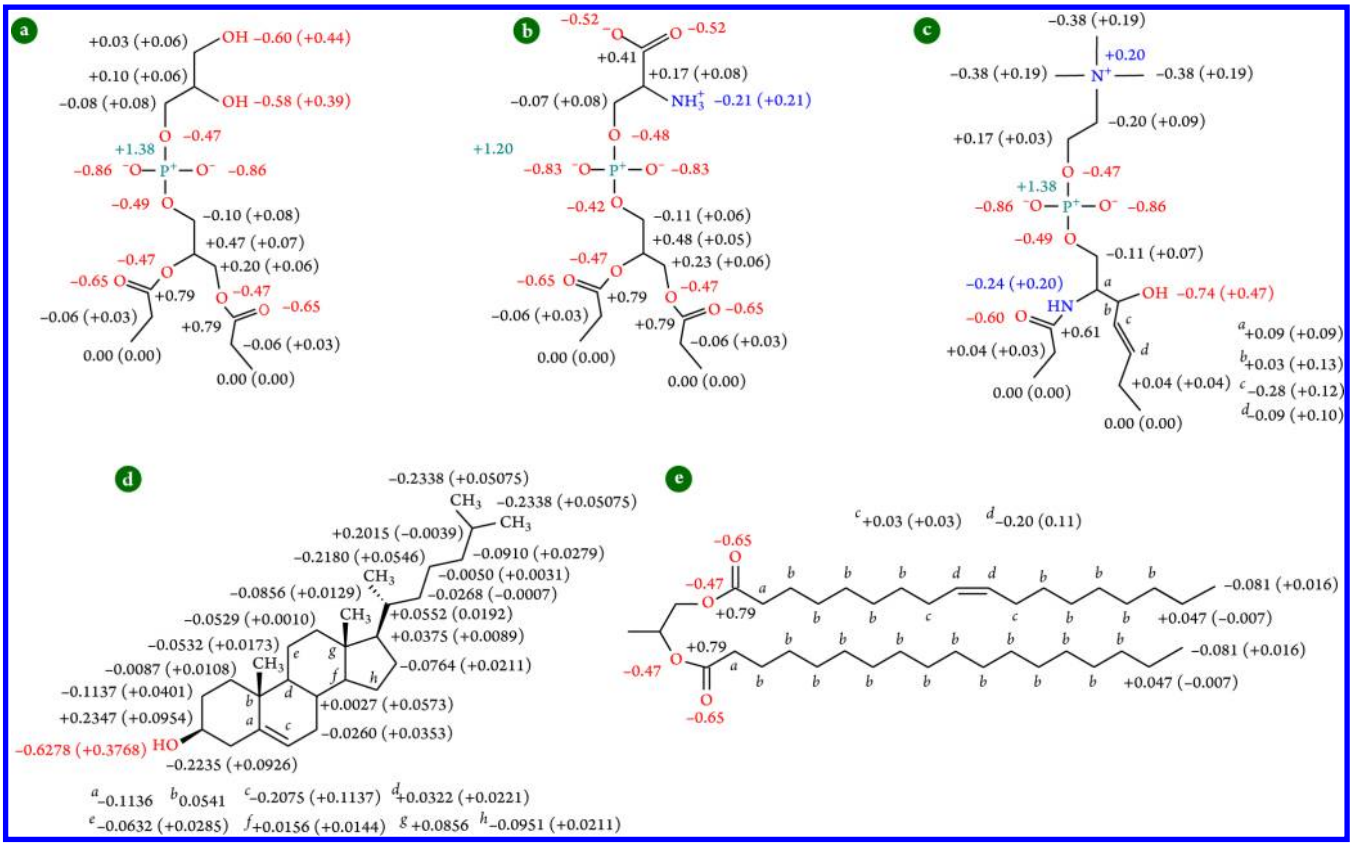

**Figure 1.** Partial atomic charges for (a) the phosphatidylglycerol headgroup, (b) the phosphatidylserine headgroup, (c) sphingomyelin lipid, (d) cholesterol, and (e) the lipid tails. All charges are given in units of proton charge. The values outside of the parentheses belong to the heavier atom, and those within parentheses belong to the hydrogen(s).

simulation is the isothermal−isobaric[48−50] since important fluctuations can be suppressed in an ensemble of constant surface tension. A number of FFs that are able to simulate lipid bilayers in the proper ensemble have been suggested[48,51−55] as well as parameters for cholesterol.[56,57] Systematic studies have also verified these findings.[58−60] We have previously developed FF parameters for saturated and unsaturated PC and PE lipids,[61,62] Slipids (Stockholm lipids), and showed their compatibility with popular FFs developed for proteins.[63−65] Most importantly, the FF was able to reproduce a number of experimental findings without applying a constant surface tension. To make Slipids more complete and versatile, we have developed parameters for SM, anionic PG, and PS lipids and cholesterol. With a more complete FF that has been developed in a consistent manner more biologically relevant systems can be studied with parameters that are highly compatible. Accurate all-atomistic models are also relevant as a basis for the so-called multiscale studies of biological systems,[39,66] which allows us to simulate larger systems on longer length and time scales. The parametrization scheme follows the previously employed one, and we focus on validating our FF against a wide range of experimental data. The resulting FF is able to describe the crucial features of fluid lipid bilayers and is very versatile, meaning that far more complex systems than just single component bilayers can be simulated with Slipids.

The remainder of the paper is organized as follows. In the Methods and Models section, the parametrization scheme and computational methods are discussed; in the Results and Discussion section, the outcome of the parametrization is analyzed by comparing a number of lipid bilayer properties to experimental data. In the last section, the most important conclusions are highlighted.

## METHODS AND MODELS

**Obtaining the Parameters.** Partial atomic charges were the main parameters that were obtained during the parametrization. Lennard-Jones (LJ) parameters as well as parameters describing covalent bonds, angles, and torsions were taken from previous Slipids parameter sets[61,62] and from the C36 FF.[53] To compute new charges for the PG and PS headgroup, initial simulations of POPG and DOPS lipid bilayers were conducted with the headgroup charges from Klauda et al.[53] The systems were equilibrated during 20 ns simulations using the same procedure as described in the following section, with the only difference being that the simulations were performed in the isothermal−isobaric ensemble with constant surface area (*NPAT*) where the area per lipid was set to the experimental values.[67,68] After equilibration, the two bilayers were simulated for 10 ns in the isothermal−isobaric (*NPT*) ensemble from which 52 random conformations per bilayer were extracted and used for the computation of partial atomic charges. The partial atomic charges were then averaged over these conformations, making them Boltzmann averaged. Sonne et al. have shown that this improves the quality of the charges,[43] and this scheme was also used for the other charges in Slipids. Only the lipid head groups and the glycerol region including the ester groups were used in the charge computations in order to save time. Charges for the ester groups were constrained to the values obtained earlier.[61] For the SM lipids, initial charges for the amide linker were


dx.doi.org/10.1021/ct300777p | J. Chem. Theory Comput. 2013, 9, 774−784

taken from the AMBER99SB FF[64] (from valine), and those for the sphingosine tail charges were taken from previous Slipids parameters and the work presented by Chiu et al.[69] The same procedure as used for the PG/PS charges was used, but keeping the charges for the headgroup fixed instead of the ester groups. As cholesterol is a more rigid molecule than lipids, charges for this stiffening molecule were computed from a single, geometry optimized, conformation which was obtained from quantum chemical calculations employing the DFT method with the B3LYP exchange-correlation functional[70−73] and the cc-pVTZ basis set.[74] In all of the computations of partial atomic charges, the B3LYP/cc-pVTZ level of theory was used with the restrained electrostatic potential (RESP) approach.[75] Solvent effects and their induced polarization of the charge distribution were effectively taken into account by placing the lipid head groups in a polarizable continuum with a dielectric constant of 78.4 with the IEFPCM model.[76,77] For cholesterol, the charges were computed in the same way but in a polarizable continuum with $\varepsilon = 2.04$ to mimic the membrane interior. All quantum mechanical calculations were performed with the Gaussian09 program suite,[78] and the RESP fitting was performed with the Red software.[79] Charges for the aliphatic chains were taken from our earlier work.[61,62] In Figure 1, all of the obtained partial atomic charges are shown. In the subsequent MD simulations all Coulombic 1−4 interactions were scaled by a factor of 0.8333 and 1−4 LJ interactions with 0.5 if no explicit interactions were assigned.

**Molecular Dynamics Simulations.** A Leap-Frog integrator was applied to integrate the equations of motion, and the LINCS algorithm[80] was used to constrain all covalent bonds, allowing a time step of 2 fs. For water, the SETTLE method was applied.[81] All simulations were performed in the *NPT* ensemble where the temperature was kept constant with the Nosé-Hoover thermostat[82,83] with water together with eventual ions and lipids coupled to separate thermostats with a coupling constant of 0.5 ps. The pressure was kept constant with a semi-isotropic scheme meaning that the pressure in the membrane plane was coupled separately from the pressure in the direction of the membrane normal. The Parrinello−Rahman barostat[84] was used to keep the pressure at one atmosphere with a coupling constant of 10 ps and a compressibility of $4.5 \times 10^{-5}$ $bar^{-1}$. Long-range electrostatic interactions with a real-space cutoff of 1.0 nm were treated by a particle mesh Ewald scheme (PME)[85,86] with a Fourier spacing of 0.12 nm and a fourth-order interpolation to the Ewald mesh. van der Waals interactions were treated with a Lennard-Jones (LJ) potential with a cutoff of 1.4 nm and a switching function from 1.4 to 1.5 nm. Long-range dispersion correction to the pressure and potential was added.[87] A twin-range cutoff scheme was used where the interactions within the short cutoff (1.0 nm) were computed every step and the interactions between the short-range cutoff and the long-range cutoff were updated every 10th step, along with the neighborlist. This treatment of long-range interactions is different from the methods explained earlier[61,62] (where a real space cutoff of 1.4 for the electrostatics was used and a single neighbor list was kept) but due to the PME treatment of the electrostatics, this does not affect the accuracy of the simulations, only the performance. Single atom based charge groups were used during the construction of the neighborlist, in agreement with all the previous parametrization and the validation of Slipids. Control simulations with a single range cutoff and with more frequent neighborlist updates (every step) were performed, and the results from these simulations validated the accuracy of our twin-range setup (data not shown). However, as this setup might be valid for bilayer systems, we urge future users that aim at studying membrane embedded proteins with Slipids to properly check their simulation protocol as it has been shown that systems other than pure bilayers are more sensitive to these manners.[88,89] Errors were estimated by using block averaging, and the atomic coordinates were saved every 1 ps.

In Table 1, all equilibrium MD simulations performed in the current manuscript are presented. To neutralize the bilayers consisting of anionic lipids, 128 sodium ions were added, described by the parameters derived by Åqvist.[90] The TIP3p water model[91] was used to hydrate the systems. For systems containing cholesterol, the total number of molecules in the bilayer was always 128. All simulated systems were equilibrated for 40 ns except for the cholesterol containing bilayers that were equilibrated for 100 ns. Production simulations were 0.5-$\mu$s-long, which gives a total of 18.5 $\mu$s of sampling. The MD simulations were performed using the Gromacs software package[92] (v. 4.5.5), and the analyses of the obtained trajectories were analyzed with the tools included in the Gromacs and MDynaMix[93] software packages. All figures of the molecular systems were rendered with VMD.[94]

**Table 1. Summary of All Equilibrium Molecular Dynamics Simulations Performed in the Present Study**

| system | temperature (K) | no. of lipids | no. of water molecules | no. of $Na^+$ ions | simulation time ($\mu$s)[a] |
|---|---|---|---|---|---|
| DLPG | 293, 303, 323, 333 | 128 | 6400 | 128 | 0.5 |
| DMPG | 303, 323, 333 | 128 | 6400 | 128 | 0.5 |
| DOPG | 293, 303, 323, 333 | 128 | 6400 | 128 | 0.5 |
| DPPG | 323, 333 | 128 | 6400 | 128 | 0.5 |
| DSPG | 333 | 128 | 6400 | 128 | 0.5 |
| POPG | 293, 303, 323, 333 | 128 | 6400 | 128 | 0.5 |
| DOPS | 303 | 128 | 6400 | 128 | 0.5 |
| 16:0 SM[b] | 323 | 128 | 5120 | 0 | 0.5 |
| 16:0 SM[c] | 323 | 120 | 4800 | 0 | 0.5 |
| 18:0 SM[d] | 323 | 128 | 5120 | 0 | 0.5 |
| DMPC[e] | 303 | 128 | 6400 | 0 | 0.5 |
| DOPC[e] | 303 | 128 | 6400 | 0 | 0.5 |
| SOPC[e] | 303 | 128 | 6400 | 0 | 0.5 |

[a]For each individual simulation. [b]Sphingomyelin 16:0. [c]With 20 mol % cholesterol. [d]Sphingomyelin 18:0. [e]With 10, 20, 30, 40, and 50 mol % cholesterol.

**Potential of Mean Force and Permeability Coefficients.** The compatibility between the TIP3p water model and Slipids was investigated by computing water permeability rates and comparing these to experiments. In order to compute the water permeability, simulations with a TIP3p water molecule constrained to certain distances from the membranes center of mass (COM) were performed. This allows for computation of the excess chemical potential or potential of mean force (PMF), $w(z)$, for transferring a water molecule across the membrane. Lipid bilayers were composed of, in total, 64 lipids (cholesterol was considered to be a lipid), and the systems were hydrated with 50 TIP3p water molecules per lipid. The following systems were investigated: DOPC with 20 and 50 mol % cholesterol, respectively, SOPC with 50 mol % cholesterol, and 18:0 SM

Table 2. Area per Lipid ($A_L$), Isothermal Area Compressibility Modulus ($K_A$), and Volume per Lipid ($V_L$) for the Simulated Bilayer Systems

| | | $A_L$ (nm$^2$) | | $K_A$ (mN m$^{-1}$) | $V_L$ (nm$^3$) | |
|---|---|---|---|---|---|---|
| lipid | temp. (K) | sim. | exptl. | sim. | sim. | exptl. |
| DLPG | 293 | 0.628 ± 0.004 | 0.634[67] | 212 ± 21 | 0.902 | 0.946[67] |
| | 303 | 0.642 ± 0.005 | 0.656[67] | 165 ± 30 | 0.922 | 0.954[67] |
| | 323 | 0.665 ± 0.005 | 0.692[67] | 147 ± 31 | 0.942 | 0.962[67] |
| | 333 | 0.679 ± 0.006 | 0.716[67] | 163 ± 37 | 0.946 | 0.971[67] |
| DMPG | 303 | 0.633 ± 0.003 | 0.651[67] | 161 ± 35 | 1.030 | 1.057[67] |
| | 323 | 0.656 ± 0.005 | 0.684[67] | 146 ± 41 | 1.052 | 1.074[67] |
| | 333 | 0.672 ± 0.006 | 0.699[67] | 179 ± 39 | 1.057 | 1.081[67] |
| DPPG | 323 | 0.645 ± 0.004 | 0.670[67] | 161 ± 27 | 1.162 | 1.189[67] |
| | 333 | 0.665 ± 0.005 | 0.694[67] | 162 ± 32 | 1.169 | 1.198[67] |
| DSPG | 333 | 0.653 ± 0.004 | 0.683[67] | 178 ± 26 | 1.279 | 1.305[67] |
| DOPG | 293 | 0.702 ± 0.005 | 0.694[67] | 210 ± 32 | 1.208 | 1.258[67] |
| | 303 | 0.708 ± 0.005 | 0.708[67] | 241 ± 36 | 1.232 | 1.265[67] |
| | 323 | 0.722 ± 0.006 | 0.729[67] | 201 ± 29 | 1.257 | 1.281[67] |
| | 333 | 0.739 ± 0.005 | 0.736[67] | 224 ± 38 | 1.264 | 1.288[67] |
| POPG | 293 | 0.656 ± 0.003 | 0.644[67] | 217 ± 30 | 1.162 | 1.210[67] |
| | 303 | 0.674 ± 0.004 | 0.661[67] | 183 ± 32 | 1.190 | 1.209[67] |
| | 323 | 0.695 ± 0.004 | 0.695[67] | 192 ± 35 | 1.210 | 1.233[67] |
| | 333 | 0.709 ± 0.006 | 0.713[67] | 188 ± 39 | 1.216 | 1.297[67] |
| DOPS | 303 | 0.641 ± 0.005 | 0.641[68] | 261 ± 27 | 1.222 | 1.228[68] |
| 16:0 SM | 323 | 0.541 ± 0.004 | | 312 ± 24 | 1.126 | |
| 18:0 SM | 323 | 0.540 ± 0.006 | 0.55[104] | 322 ± 38 | 1.181 | |

with 50 mol % cholesterol. To obtain starting structures, every system was run for 200 ns of unbiased simulations, and the final snapshots from these simulations were then used in the subsequent constrained simulations. The reaction coordinate for the constrained simulations was the distance between the COM of one water molecule and the bilayer along the membrane normal ($z$-direction). The COM of the bilayer was defined as $z = 0$. Initially, one water molecule was placed at the desired position, and the interactions between this molecule and the rest of the system were gradually switched on during a 10 ns long simulation. The final snapshot from these simulations was then used for production simulations. The positions along the $z$-direction were separated by 0.1 nm, and 80 constrained simulations were performed for each system. Sampling of each position along the membrane normal was performed for 30 ns excluding the initial 10 ns, which was considered as equilibration, summing up to a to total sampling time of 12.8 $\mu$s. Other simulation parameters were identical to the ones presented in the previous section.

PMFs were constructed from the forces acting on the water molecule in question

$$w(z) = -\int_{z_0}^{z} \langle F(z') \rangle \, dz' \tag{1}$$

where $\langle F(z') \rangle$ is the mean force acting on the water molecule at a bilayer depth of $z'$. The integration was performed from the bulk water phase over the membrane. The local diffusion coefficient can be computed according to[95−97]

$$D_z(z) = \frac{(RT)^2}{\int \langle \Delta F_z(t) \, \Delta F_z(0) \rangle \, dt} \tag{2}$$

where $R$ is the gas constant, $T$ is the absolute temperature, and $\langle \Delta F_z(t) \; \Delta F_z(0) \rangle$ is the autocorrelation function of the deviation from the mean force. $\Delta F_z(t)$ is defined as

$$\Delta F_z(t) = F_z(t) - \langle F_z \rangle \tag{3}$$

The autocorrelation function of the force deviation was fitted to the following function in order to perform the integration:

$$f_{ACF} = A \, e^{-t/\tau_0} + B \, e^{-t/\tau_1} \tag{4}$$

From the above stated equations, the permeability coefficient can be calculated and compared to experimental data according to[97]

$$\frac{1}{P} = \int_{z_1}^{z_2} \frac{e^{w(z)/RT}}{D_z(z)} \, dz \tag{5}$$

where $z_1 = -3$ nm and $z_2 = 3$ nm; i.e., the integration was carried out over the whole lipid bilayer. Errors were estimated using block averaging with 5 ns blocks.

## RESULTS AND DISCUSSION

**Single Component Bilayers.** *Area and Volume per Lipid.* In Table 2, areas per lipid ($A_L$) for the PG and SM lipid bilayers are presented. $A_L$ was calculated by projecting the area of the simulation box in the $xy$-plane onto the lipids, an approximation that works well for smaller membrane patches.[98] Slipids systematically underestimates $A_L$ for the PG lipids with saturated tails, especially at temperatures equal to or higher than 323 K. The contraction of the charged, fully saturated lipids is in agreement with previous findings of Gurtovenko et al.[99] and Miettinen et al.[100] Despite the underestimation of $A_L$, none of the studied systems undergo a phase transition; i.e., all bilayers are in the $L_\alpha$ phase. For lipids with one or two double bonds, the agreement with experiments is, however, excellent. A possible reason for the disagreement between simulations and experiments could be the differences in ion concentrations: in the simulations presented here, sodium ions were added to neutralize the systems, whereas in the experimental studies NaCl is added in addition to the $Na^+$/PG mixture. It has been


dx.doi.org/10.1021/ct300777p | J. Chem. Theory Comput. 2013, 9, 774−784

shown in simulations of bilayers together with ions that the structure of the membrane is altered by ion binding.[101] However, it should be mentioned that the effects of ions on membranes in MD simulations are sensitive to the FF used for the ions,[102,103] so more experimental data are needed in order to judge the quality and the compatibility of membrane and ion FFs.

The available experimental data for SM lipids are rather limited, which makes validation of the results presented in Table 2 inconclusive. For 18:0 SM, there is an agreement between experiments and simulations, but it should be mentioned that the value reported by Maulik et al.[104] is based on the assumption that the volume per lipid for 18:0 SM is the same as that for DPPC. Chiu et al.[69] estimated the area of 18:0 SM to be 0.527 nm$^2$ when using a volume per lipid nearly identical to the one reported here. For the shorter SM lipid, 16:0 SM, $A_L$ is slightly larger than the values that can be found in the literature from earlier simulations with different FFs.[105−107] As $A_L$ is difficult to measure,[6] it has been suggested that this property alone is not a proper indicator of the accuracy of a simulation.[58,108] In the following sections, we compute properties that are less ambiguous to determine from experiments.

From the fluctuations in $A_L$, the isothermal area compressibility modulus ($K_A$) can be determined according to

$$K_A = \frac{2A_L}{\beta n_L \sigma_A^2} \tag{6}$$

where $\beta = 1/k_BT$, $n_L$ is the number of lipids, and $\sigma_A{}^2$ is the variance of $A_L$. No experimental data are available (as far as we know) for $K_A$, but when compared to values for saturated and mono-/di-unsaturated PC lipids modeled by Slipids,[61,62] it is clear that the PG lipids are easier to compress.

The volume per lipid ($V_L$) was calculated according to

$$V_L = \frac{\langle V_{box} \rangle - n_W V_W}{n_L} \tag{7}$$

where $\langle V_{box} \rangle$ is the average volume of the simulation box, $n_W$ is the number of water molecules in the bilayer system, and $V_W$ is the volume per water molecule (determined from simulations of pure TIP3p water). In Table 2, $V_L$ values from simulations are compared to experiments. All volumes are slightly underestimated, in accordance with our previous work; however, the underestimation is less pronounced for the PG lipids than for PC/PE lipids.[61,62] As before, we believe that this discrepancy is due to the headgroup parameters. Different ion conditions in our simulations and experiments may also play a role.

*Membrane Thickness.* Two types of thicknesses were computed: the head-to-head distance ($D_{HH}$) and the Luzzati thickness ($D_B$). The former is simply the distance between the two peaks in an electron density profile and can be accessed via X-ray scattering experiments due to the electron-rich regions in the lipid head groups. $D_B$ is defined as[109,110]

$$D_B = d_z - \int_{-d_z/2}^{d_z/2} \rho_W(z)\, dz \tag{8}$$

where $d_z$ is the dimension of the simulation box in the $z$ direction and

$$\rho_W(z) = \frac{n_W V_W}{dV} \tag{9}$$

which is the time-averaged histogram of the water distribution along the membrane normal. $n_W$ is the (time) average of the number of water molecules per slice, and $dV$ is the average volume of the slice. In Table 3, these two values are presented.

**Table 3. Luzzati Thickness ($D_B$) and Head-to-Head Distance ($D_{HH}$) from Simulations and Various Experiments[a]**

| | | $D_B$ | | $D_{HH}$ | |
|---|---|---|---|---|---|
| lipid | temp. (K) | sim. | exptl. | sim. | exptl. |
| DLPG | 293 | 2.92 | 2.99[67] | 3.16 | |
| | 303 | 2.90 | 2.91[67] | 2.70 | |
| | 323 | 2.88 | 2.78[67] | 2.74 | |
| | 333 | 2.87 | 2.72[67] | 2.76 | |
| DMPG | 303 | 3.24 | 3.25[67] | 3.18 | |
| | 323 | 3.22 | 3.14[67] | 3.05 | |
| | 333 | 3.20 | 3.09[67] | 3.02 | |
| DPPG | 323 | 3.62 | 3.55[67] | 3.49 | |
| | 333 | 3.54 | 3.45[67] | 3.40 | |
| DSPG | 333 | 3.83 | 3.82[67] | 3.80 | |
| DOPG | 293 | 3.53 | 3.63[67] | 3.42 | |
| | 303 | 3.50 | 3.57[67] | 3.45 | |
| | 323 | 3.48 | 3.51[67] | 3.36 | |
| | 333 | 3.34 | 3.50[67] | 3.34 | |
| POPG | 293 | 3.69 | 3.73[67] | 3.60 | |
| | 303 | 3.68 | 3.66[67] | 3.54 | 3.73[111] |
| | 323 | 3.60 | 3.55[67] | 3.39 | |
| | 333 | 3.50 | 3.49[67] | 3.36 | |
| DOPS | 303 | 3.85 | 3.83[68] | 3.81 | 3.90[68] |
| 16:0 SM | 323 | 4.10 | | 4.22 | 4.44[112] |
| 18:0 SM | 323 | 4.45 | | 4.26 | 4.1[104] |

[a]All values are shown in nm.

Only a few experimental values are available for $D_{HH}$, and the simulations agree well with these values. For $D_B$, experimental data are available, and the small differences between the simulations and these data show that Slipids is able to capture the balance between hydrophilicity and hydrophobicity of the lipid molecules. The thermal dependency of these simulated properties is also well reproduced.

*NMR Order Parameters.* From simulations the deuterium order parameters can be obtained via the following expression:

$$S_{CD} = \frac{1}{2}\langle 3\cos^2\theta - 1 \rangle \tag{10}$$

where $\theta$ is the angle between the C−H dipole and the bilayer normal. When $S_{CD} = 0$, the hydrocarbon chains are in random orientations, or at an orientation corresponding to the "magic angle" (∼54°) between the C−H vector and the membrane normal. If $S_{CD} = -0.5$, they are aligned in perfect *trans* conformations along the membrane normal. $S_{CD}$ is an experimental key property to compare simulations to since NMR methods used to obtain this parameter are reliable and free from interpretations. As shown in Figure 2, the ordering for the acyl chain of 16:0 SM is slightly too high when compared to experiments. However, the values obtained from the simulations here are close to values reported from other simulation studies.[105−107]

*X-Ray Scattering Form Factors.* X-ray scattering form factors ($F(q)$) are ideal properties to compare simulations to because these are directly measurable experimental properties.[7,110,114,115] From simulations, $F(q)$ can be obtained by

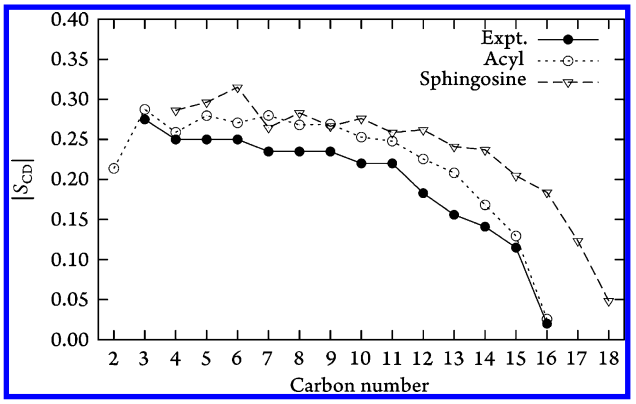


**Figure 2.** Order parameters for 16:0 sphingomyelin at 323 K compared to experimental findings for the acyl chain.[113]

performing a Fourier transformation of the electron density profile along the membrane normal

$$F(q) = \int_{-d_z/2}^{d_z/2} (\rho_{el}(z) - \rho_{el}^{W}(z)) \cos(qz)\, dz \quad (11)$$

where $\rho_{el}(z)$ is the electron density at position $z$ and $\rho_{el}^{W}(z)$ is the electron density of bulk water. In Figure 3, $F(q)$'s from

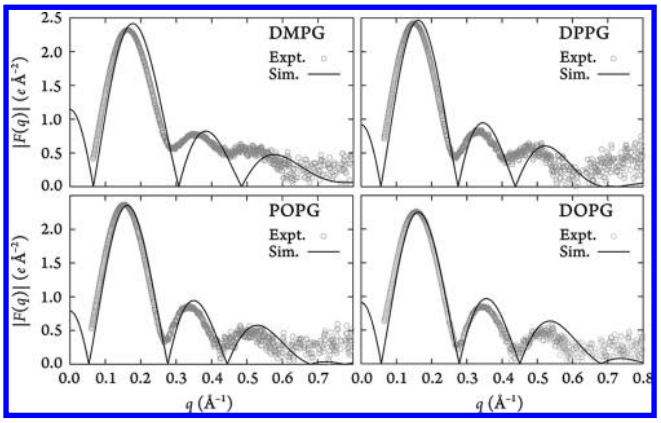


**Figure 3.** X-ray scattering form factors for lipids with phosphatidylglycerol head groups. All form factors are reported at 303 K for DMPG, POPG, and DOPG and 323 K for DPPG. Experimental data are from Pan et al.[67]

simulations are compared to experimental data for PG lipids. The relative peak height is reproduced with slight deviations, and the minima coincide with the experimental data. This indicates that the bilayers have the correct structure along the direction of the bilayer normal, and it is likely any further structural data obtained from these trajectories are reliable. As lipid bilayers behave as fluids in two dimensions and are more or less structured along the membrane normal, it is difficult to makes claims regarding the behavior of the bilayer in the other two perpendicular directions. The small deviations could be attributed to the differences in $A_L$ as noted by Kučerka et al.[111] The nonzero minima observed in experiments for DMPG and DPPG could indicate a possible asymmetry of the bilayers in the experimental setup.[115]

**Binary Mixtures of Lipids and Cholesterol.** *Local Chain Ordering.* The well-known condensing and stiffening effect of cholesterol on lipid bilayers[14−16,18−20] is evident from the MD simulations performed here. As the lateral area of the bilayer shrinks, the acyl chains packs closer around cholesterol, and the general ordering of the membrane naturally increases. This behavior can be described by the order parameters. In Figure 4, order parameters for four different bilayers containing cholesterol are presented. Generally the ordering is much more pronounced than in cholesterol-free bilayers (compare e.g. Figure 2 and Figure 4). For DMPC, the simulations agree well with experiments, indicating that the local structure along

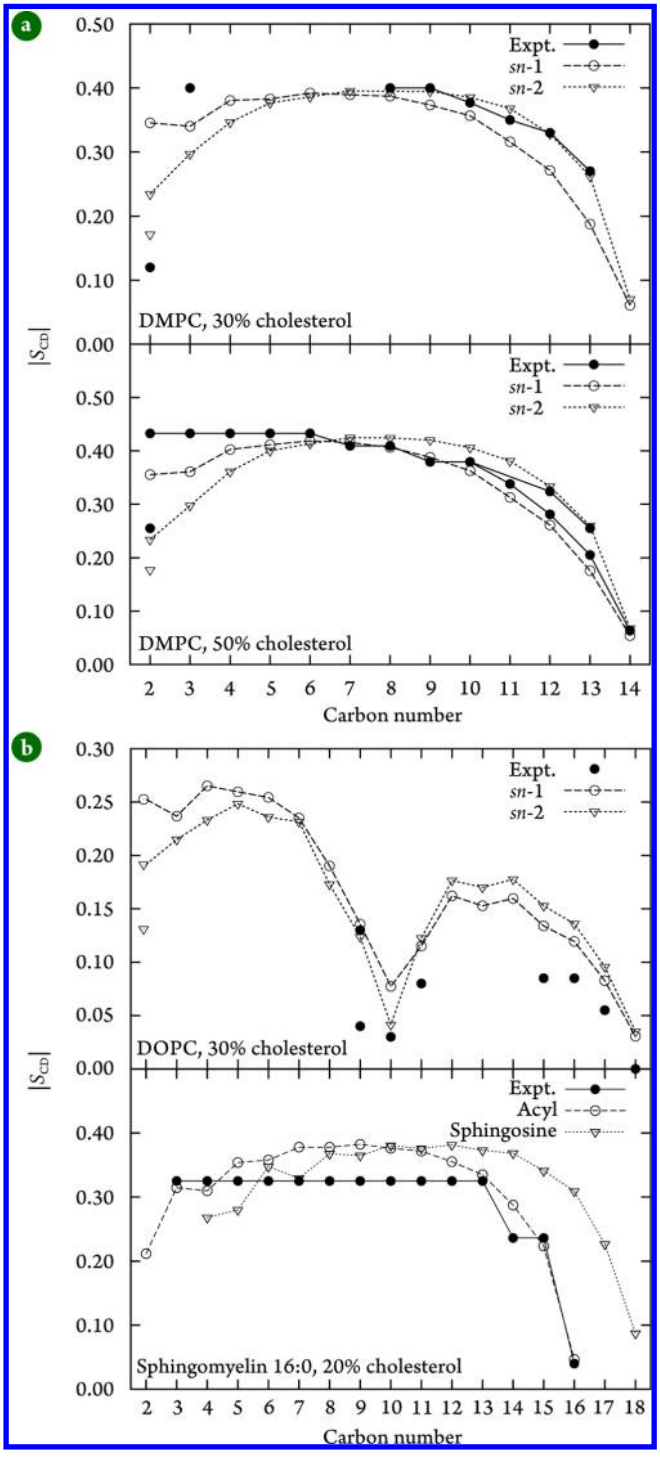


**Figure 4.** NMR order parameters for (*a*) DMPC/cholesterol mixtures with different composition compared to the experimental values of Vermeer et al.[116] (30%) and Trouard et al.[119] and (*b*) a DOPC/cholesterol and a sphingomyelin/cholesterol mixture compared to NMR studies by Warschawski and Devaux[18] and Bartels et al.[113]


dx.doi.org/10.1021/ct300777p | J. Chem. Theory Comput. 2013, 9, 774−784

the membrane normal of the lipids are correctly described by the parameter set proposed here. Closer to the bilayer center, there is a slight difference in ordering of the *sn*-1 and *sn*-2 tails, but closer to the region where the cholesterol rings are located, the difference vanishes. The splitting of the order parameters for the second carbon of the *sn*-2 chain is present in all phospholipid simulations and in agreement with experimental data. This splitting has been difficult to obtain for simulations performed with united-atom FFs for bilayers containing cholesterol.[116] When cholesterol is embedded in a bilayer containing double bonds, like a DOPC bilayer, the increase in ordering is not as evident as for the saturated lipids (Figure 4b, top). The order parameter of the 10th carbon of the chain is hardly affected by presence of cholesterol when comparing experimental[18] and simulation[62,117] data. A nearly zero order parameter like this can be explained by the preference of the $C_{10}$−H dipole vector close to the "magic angle" with respect to the membrane normal. Martinez-Seara et al.[118] also observed a higher fluidity of bilayers with unsaturated lipids and cholesterol when the double bond is positioned in the middle of the hydrophobic tail (which is the case for DOPC). As for DOPC, the agreement with experiments for the 16:0 SM/cholesterol bilayer is worse than for the binary DMPC/cholesterol mixtures. However, the order parameters are close to the recent published values of Metcalf and Pandit.[105] The plateau in the experimental data indicates a lack of resolution and specific assignments, which makes the comparison with these values not as optimal as in our previous comparisons.[61,62] The values presented in the present manuscript are slightly lower than previously reported from other simulations employing other FFs.[23,117] As can be seen further on, the agreement between X-ray form factors from our simulations and experiments is evident for binary mixtures of DOPC/cholesterol. On the basis of this, we can conclude that we indeed are able to describe the features of the two-component system accurately.

The orientation of cholesterol in lipid bilayers is also important, and in Figure 5 order parameters for different C−H

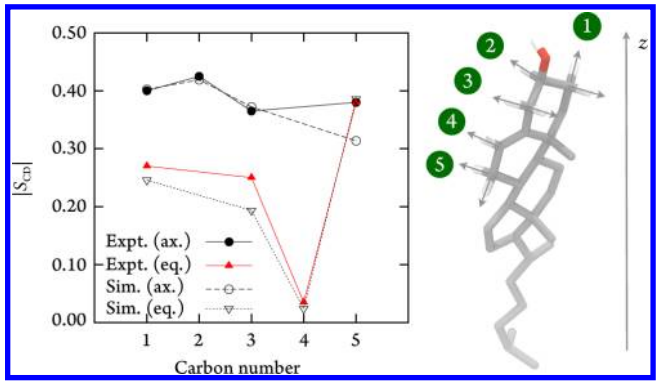


**Figure 5.** Order parameters for axial and equatorial C−H dipoles in cholesterol compared to experiments[116] for a DMPC lipid bilayer with 30 mol % cholesterol.

bonds in the ring region of cholesterol are compared to experimental data.[116] The agreement is satisfactory albeit not excellent; however, the errors are very small when converting $|S_{CD}|$ into degrees. It is clear that cholesterol is almost aligned perfectly with the bilayer normal.

*Mechanical Properties and Thickness.* As the concentration of cholesterol increases, it is intuitive that the isothermal area compressibility modulus should increase. In experiments, it has been seen that $K_A$ more than doubles when the amount of cholesterol is increased from 30 to 50 mol %.[29,120] In Table 4,

**Table 4. Isothermal Area Compressibility for Binary Mixtures of Different Composition**

| | | $K_A$ (mN m$^{-1}$) | |
|---|---|---|---|
| lipid | mol% cholesterol | sim. | exptl. |
| DMPC | 30 | 585 ± 0.17 | |
| | 50 | 1735 ± 14 | |
| DOPC | 30 | 343 ± 19 | 420[29] |
| | 50 | 677 ± 21 | 870[120] |
| SOPC | 30 | 318 ± 16 | 430[29] |
| | 50 | 1183 ± 11 | 1130[120] |

values from simulations are compared to these experimental findings. Our simulations are able to capture this decrease in compressibility, although the absolute values are slightly underestimated except in the case of a 1:1 mixture of SOPC and cholesterol. In agreement with the findings of Pan et al.[29] and general belief, cholesterol has the most pronounced effect on the mechanical properties of fully saturated lipids. Biological membranes can alter their mechanical properties by controlling the amount of cholesterol and how, e.g., lipid rafts alter the behavior of cell membranes in terms of mechanical properties such as $K_A$, and the bending modulus can, in principle, be studied with the parameters presented here.

Since cholesterol has a condensing effect on bilayers, the *trans*/*cis* ratio is increasing. As the number of *gauche* kinks are decreased, the bilayer is increasing in thickness. This is illustrated in Figure 6 where $D_{HH}$ is shown as a function of

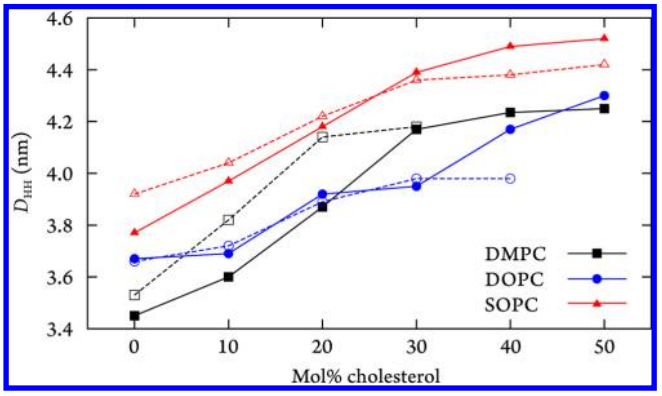


**Figure 6.** Bilayer head-to-head distances ($D_{HH}$) as a function of cholesterol content. Data from simulations are shown with filled points and solid lines, and experimental data[29] are shown as unfilled points with dashed lines.

cholesterol concentration. For lower concentrations (<30 mol %), the increase in thickness is dramatic, and beyond this concentration, the bilayer thickness changes to a lesser extent. Agreement with experiments is clear for DOPC and SOPC but less evident for DMPC at lower concentrations. The reason for this discrepancy can be a matter for further investigation.

*X-Ray Scattering Form Factors.* In Figure 7, computed X-ray scattering form factors are compared to experimental data. Since X-rays give high contrast between electron rich domains, e.g. phosphate groups, and less electron rich domains, e.g. acyl chains, structural refinements between these groups can be

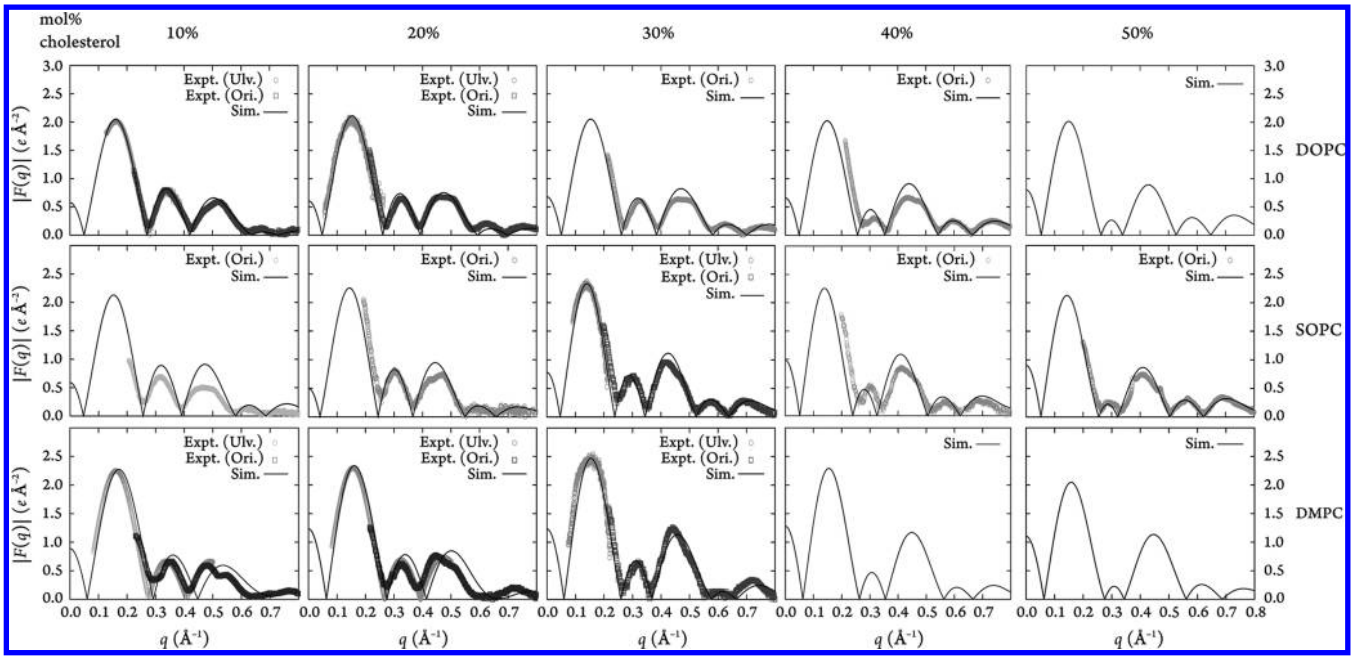


**Figure 7.** X-ray scattering form factors for DOPC (top), SOPC (middle), and DMPC (bottom) lipid bilayers with varying cholesterol content compared to experiments.[28,29,121,122]

obtained from experiments. Since the data obtained from the simulations agree well with the experimental data, we can conclude that Slipids is able to reproduce important structural features of these binary systems. All minima are moved toward smaller $q$ values with increasing cholesterol concentration, which indicates that the bilayers are indeed getting thicker. Furthermore, both the width and the relative height of the second lobe is decreased and the lobes at larger $q$-values are becoming more evident with an increasing cholesterol amount. This is an indication of a change in the bilayer at distances closer to the bilayer center. Consistent with the discrepancy in bilayer thickness, the agreement between simulations and experiments for DMPC at 10 and 20 mol % is not as prominent as for the other studied systems. Since $|F(q)|$ is sensitive to the bilayer thickness, this is a rather expected result. It is however safe to say that the cholesterol parameters are highly compatible with previous parameters obtained for phospholipids with different degrees of saturation. At higher cholesterol concentrations for DMPC and for all concentration in DOPC/SOPC, the agreement with experiments is excellent.

*Water Permeability.* In Figure 8, the PMF for transferring a TIP3p water molecule across a lipid bilayer with various amounts of cholesterol is presented. As the cholesterol amount is increased, the free energy barrier for water insertion is enhanced. The biggest impact is seen at depths between 0.8 and 1.5 nm, which also is the region where most of the cholesterol resides. For the 1:1 mixture of 18:0 SM and cholesterol, the barrier is the highest, and this can probably be attributed to the lowest $A_L$ (Table 5), which is in agreement with both experiments[123] and simulations.[31,32] The effects of cholesterol are also the least pronounced for the DOPC/cholesterol mixture. Together, these findings confirm the results of Wennberg et al.,[31] who saw that the effects on permeability are most dramatic for saturated lipids. As SOPC only has one double bond, it is between DOPC and 18:0 SM in terms of unsaturation, and the PMF for the 1:1 SOPC/cholesterol mixture should lie in between the PMFs for the 1:1

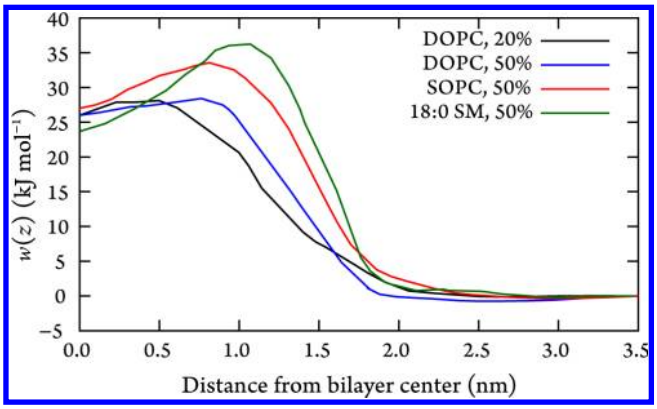


**Figure 8.** Potentials of mean force for transferring a TIP3p water molecule from the bulk phase to the bilayer center. Percentage numbers indicate the mol % of cholesterol.

**Table 5. Water Permeability ($P_w$) and Area per Lipid ($A_L$) for Two Component Membranes**[a]

| bilayer | temperature (K) | $P_w$ ($10^{-3}$ cm s$^{-1}$) sim. | $P_w$ ($10^{-3}$ cm s$^{-1}$) exptl. | $A_L$ (nm$^2$)[b] |
|---|---|---|---|---|
| DOPC (20) | 303 | 3.2 ± 0.6 | 11.5 ± 0.58[123] | 0.57 ± 0.005 |
| DOPC (50) | 303 | 1.8 ± 0.4 | 0.58 ± 0.06,[120c] | 0.43 ± 0.004 |
| SOPC (50) | 303 | 0.2 ± 0.1 | 0.64 ± 0.13[120] | 0.41 ± 0.003 |
| 18:0 SM (50) | 303 | 0.2 ± 0.1 | 0.39 ± 0.1[120] | 0.39 ± 0.003 |

[a]Values within parentheses indicate the amount of cholesterol in mol %. [b]$A_L = A_{xy}/(n_{lipid} + n_{cholesterol})$. [c]288 K.

DOPC/cholesterol and the 18:0 SM/cholesterol mixtures, which it does in Figure 8. The reason for this is believed to be the interaction between the saturated lipid chains and cholesterol. As these interactions are stronger than the


dx.doi.org/10.1021/ct300777p | J. Chem. Theory Comput. 2013, 9, 774−784

interactions between cholesterol and unsaturated lipid chains, the enthalpy related penalty for breaking the former interactions is larger than for breaking the latter.[31] The preference of cholesterol for SM lipids over unsaturated lipids has also been observed by Aittoniemi et al.[124]

From eq 5, the permeability rates of water through the different binary mixtures were calculated, and the results are presented in Table 5. Simulations performed with Slipids systematically underestimates the permeability rates but all values are on the same order of magnitude as the experiments. As the diffusion of the TIP3p water model is faster than observed experimentally,[125,126] this might appear to be contradictory. The reason for this discrepancy with experiments can then have three possible explanations: (1) the interactions between Slipids lipids and the TIP3p water model are not well-tuned, (2) the systems studied in our simulations differ from the systems studied in experiments, or (3) it may be related to the approximations involved in the definition of permeability according to eq 2−5. The first explantation seems unlikely since this would have been reflected in other membrane properties presented here ($A_L$, $D_B$, $F(q)$, etc.). The second explanation is therefore more plausible. As pointed out by Wennberg et al.,[31] systems used in simulations differ from the macroscopic membranes that are used in simulations, where spatial fluctuations of cholesterol are much more pronounced. Due to the limited system sizes in MD simulations, the permeability through cholesterol rich regions is only accounted for, whereas in experiments it is very likely that regions which are depleted of cholesterol contribute the most to the permeability.

## CONCLUSIONS

The Slipids FF has now been extended to include vital parts of biological membranes such as SM, PG, and PS lipids and cholesterol. As the surface tension of a biological membrane is zero,[49] it is important to have empirical potentials available for MD simulations that can be used in the *NPT* ensemble where the membrane is allowed to laterally expand and contract. These fluctuations will be of importance in embedding studies of peptides, proteins, and smaller solutes in lipid bilayers. The careful validation performed here shows that the parameters are able to reproduce important structural properties of single and double component membranes without applying a surface tension. Besides properties like membrane thickness, order parameters, and form factors being in excellent agreement with available experimental data, water permeability in binary membranes has also been proven to agree relatively well with experiments.

As all parameters have been developed in a consistent manner, more complex systems that include both proteins and different lipids can be studied in an accurate and effective manner on a microsecond time scale.

## ASSOCIATED CONTENT

### Supporting Information

A zip archive with topologies ready for use with the Gromacs software package as well as force field parameters and coordinates for equilibrated lipid bilayers (also available at http://people.su.se/~jjm). This material is available free of charge via the Internet at http://pubs.acs.org/.

## AUTHOR INFORMATION

### Corresponding Author

*E-mail: joakim.jambeck@mmk.su.se, jambeck@me.com. E-mail: alexander.lyubartsev@mmk.su.se

### Notes

The authors declare no competing financial interest.

## ACKNOWLEDGMENTS

This research has been supported by the Swedish Research Council, grant no. 621-2010-5005. The simulations were performed on resources provided by the Swedish National Infrastructure for Computing (SNIC-003-11-3), at PDC Center for High Performance Computing, High Performance Computing Center North (HPC2N), and National Supercomputer Centre (NSC). We thank A. Rabinovich for fruitful discussions and J. F. Nagle, N. Kučerka, and G. Khelashvili for providing experimental data. This work makes use of results produced by the ScalaLife project, a project cofunded by the European Commission (under contract number INFSO-RI-261523). More information on ScalaLife is available at http://www.scalalife.eu. The reviewers are thanked for contributing with constructive criticism.

## REFERENCES

(1) Tieleman, D. P.; Berendsen, H. J. C. *J. Chem. Phys.* **1996**, *105*, 4871−4880.
(2) Tieleman, D. P.; Marrink, S. J.; Berendsen, H. J. C. *Biochim. Biophys. Acta* **1997**, *1331*, 235−270.
(3) Lindahl, E.; Edholm, O. *Biophys. J.* **2000**, *79*, 426−433.
(4) Högberg, C.-J.; Nikitin, A. M.; Lyubartsev, A. P. *J. Comput. Chem.* **2008**, *29*, 2359−2369.
(5) Nagle, J. F.; Tristram-Nagle, S. *Biochim. Biophys. Acta* **2000**, *1469*, 159−195.
(6) Nagle, J. F.; Tristam-Nagle, S. *Curr. Opin. Struct. Biol.* **2000**, *10*, 474−480.
(7) Kučerka, N.; Liu, Y.; Chu, N.; Petrache, H. I.; Tristram-Nagle, S.; Nagle, J. F. *Biophys. J.* **2005**, *88*, 2626−2637.
(8) Takamori, S.; et al. *Cell* **2006**, *127*, 831−846.
(9) Wu, N. A. N.; Palczewski, K.; Mu, D. J. *Pharmacol. Rev.* **2008**, *60*, 43−78.
(10) Simons, K.; Ikonen, E. *Nature* **1997**, *70*, 270−572.
(11) Brown, D. A.; London, E. *Annu. Rev. Cell Dev. Biol.* **1997**, *14*, 111−136.
(12) Ahmed, S. N.; Brown, D. A.; London, E. *Biochemistry* **1997**, *36*, 10944−10953.
(13) Contreras, F. X.; Ernst, A. M.; Haberkant, P.; Björkholm, P.; Lindahl, E.; Gönen, B.; Tischer, C.; Elofsson, A.; von Heijne, G.; Thiele, R.; Pepperkok, C.; Wieland, F.; Brügger, B. *Nature* **2012**, *481*, 525−529.
(14) Ikonen, E. *Nat. Rev. Mol. Cell. Biol.* **2008**, *9*, 125−138.
(15) Nezil, F. A. *Biophys. J.* **1992**, *61*, 1176−1183.
(16) Martinez, G. V.; Dykstra, E. M.; Lope-Piedrafita, S.; Job, C.; Brown, M. F. *Phys. Rev. E* **2002**, *66*, 050902.
(17) Hofsäß, C.; Lindahl, E.; Edholm, O. *Biophys. J.* **2003**, *84*, 2196−2206.
(18) Warschawski, D.; Devaux, P. *Eur. Biophys. J.* **2005**, *34*, 987−996.
(19) Purdy, P.; Fox, M.; Graham, J. *Cryobiology* **2005**, *51*, 102−112.
(20) Hung, W.; Lee, M.; Chen, F.; Huang, H. W. *Biophys. J.* **2007**, *92*, 3960−3967.
(21) Róg, T.; Pasenkiewicz-Gierulab, M.; Vattulainen, I.; Karttunen, M. *Biochim. Biophys. Acta* **2009**, *1788*, 97−121.
(22) Edholm, O.; Nagle, J. F. *Biophys. J.* **2005**, *89*, 1827−1832.
(23) Alwarawrah, M.; Dai, J.; Huang, J. *J. Phys. Chem. B* **2010**, *114*, 7516−7523.
(24) Kuwabara, P. E.; Labousse, M. *Trends Genet.* **2002**, *18*, 193−201.
(25) Epand, R. M. *Prog. Lipid Res.* **2006**, *45*, 279−294.

(26) Ollila, O. H. S.; Róg, T.; Karttunen, M.; Vattulainen, I. *J. Struct. Biol.* **2007**, *159*, 311−323.
(27) Kaiser, H. J.; Or, A.; Róg, T.; Nyholm, T. K. M.; Chai, W.; Feizi, T.; Lingwood, D.; Vattulainen, I.; Simons, K. *Proc. Natl. Acad. Sci. U. S. A.* **2011**, *108*, 16628−16633.
(28) Pan, J.; Mills, T. T.; Tristam-Nagle, S.; Nagle, J. *Phys. Rev. Lett.* **2008**, *100*, 198103.
(29) Pan, J.; Tristam-Nagle, S.; Nagle, J. F. *Phys. Rev. E* **2009**, *80*, 021931.
(30) Eriksson, E. S. E.; Eriksson, L. A. *J. Chem. Theory Comput.* **2011**, *7*, 560−574.
(31) Wennberg, C. L.; van der Spoel, D.; Hub, J. S. *J. Am. Chem. Soc.* **2012**, *134*, 5351−5361.
(32) Saito, H.; Shinoda, W. *J. Phys. Chem. B* **2011**, *115*, 15421−15250.
(33) Ridder, A. N. J. A.; Kuhn, A.; Killian, J. A.; de Kruijff, B. *EMBO Rep.* **2001**, *21*, 403−408.
(34) Poolman, B.; Spitzer, J. J.; Wood, J. M. *Biochim. Biophys. Acta* **2004**, *1666*, 88−104.
(35) Kimura, T.; Yeliseev, A. A.; Vukoti, K.; Rhodes, S. D.; Cheng, K.; Rice, K. C.; Gawrisch, K. *J. Biol. Chem.* **2012**, *287*, 4076−4087.
(36) Lyubartsev, A. P.; Rabinovich, A. L. *Soft Matter* **2011**, *7*, 25−39.
(37) Gumbart, J.; Wang, Y.; Aksimebtiev, A.; Tajkhorshid, E.; Schulten, K. *Curr. Opin. Struct. Biol.* **2005**, *15*, 423−431.
(38) Lindahl, E.; Sansom, M. S. P. *Curr. Opin. Struct. Biol.* **2008**, *18*, 425−431.
(39) Stansfeld, P. J.; Sansom, M. S. P. *Structure* **2012**, *19*, 1562−1572.
(40) Vivcharuk, V.; Tomberli, B.; Tolokh, I. S.; Gray, C. G. *Phys. Rev. E* **2008**, *77*, 031913.
(41) Tolokh, I. S.; Vivcharuk, V.; Tomberli, B.; Gray, C. G. *Phys. Rev. E* **2009**, *80*, 031911.
(42) Hyvönen, M. T.; Kovanen, P. T. *Eur. Biophys. J.* **2005**, *34*, 294−305.
(43) Sonne, J.; Jensen, M. O.; Hansen, F. Y.; Hemmingsen, L.; Peters, G. *Biophys. J.* **2007**, *92*, 4157−4167.
(44) Siu, S. W. I.; Vácha, R.; Jungwirth, P.; Böckmann, R. A. *J. Chem. Phys.* **2008**, *128*, 125103.
(45) Jójart, B.; Martinek, T. A. *J. Comput. Chem.* **2007**, *28*, 2051−2058.
(46) Rosso, L.; Gould, I. R. *J. Comput. Chem.* **2008**, *29*, 24−37.
(47) Taylor, J.; Whiteford, N. E.; Bradley, G.; Watson, G. W. *Biochim. Biophys. Acta* **2009**, *1788*, 638−649.
(48) Berger, O.; Edholm, O.; Jähnig, F. *Biophys. J.* **1997**, *72*, 2002−2013.
(49) Jähnig, F. *Biophys. J.* **1996**, *71*, 1348−1349.
(50) Marrink, S. J.; Mark, A. E. *J. Phys. Chem. B* **2001**, *105*, 6122−6172.
(51) Kukol, A. *J. Chem. Theory Comput.* **2009**, *5*, 615−626.
(52) Ulmschneider, J. P.; Ulmschneider, M. B. *J. Chem. Theory Comput.* **2009**, *5*, 1803−1813.
(53) Klauda, J. B.; Venable, R. M.; Freites, J. A.; O'Connor, J. W. O.; Tobias, D. J.; Mondragon-Ramirez, C.; Vorobyov, I.; MacKerell, A. D., Jr.; Pastor, R. W. *J. Phys. Chem. B* **2010**, *114*, 7830−7843.
(54) Poger, W. F.; van Gunsteren, D.; Mark, A. E. *J. Comput. Chem.* **2010**, *31*, 1117−1125.
(55) Dickson, C. J.; Rosso, L.; Betz, R. M.; Walker, R. C.; Gould, I. R. *Soft Matter* **2012**, *8*, 9617−9627.
(56) Höljte, M.; Förster, T.; Brandt, B.; Engels, T.; von Rybinski, W.; Höljte, H. D. *Biochim. Biophys. Acta* **2001**, *1511*, 156−167.
(57) Lim, J. B.; Rogaski, B.; Klauda, J. B. *J. Phys. Chem. B* **2012**, *116*, 203−210.
(58) Poger, D.; Mark, A. E. *J. Chem. Theory Comput.* **2010**, *6*, 325−336.
(59) Piggot, T. J.; Piñeiro, A.; Khalid, S. *J. Chem. Theory Comput.* **2012**, [ASAP] DOI: 10.1021/ct3003157.
(60) Poger, D.; Mark, A. E. *J. Chem. Theory Comput.* **2012**, [ASAP] DOI: 10.1021/ct300675z.
(61) Jämbeck, J. P. M.; Lyubartsev, A. P. *J. Phys. Chem. B* **2012**, *116*, 3164−3179.
(62) Jämbeck, J. P. M.; Lyubartsev, A. P. *J. Chem. Theory Comput.* **2012**, *8*, 2938−2948.
(63) Duan, Y.; Wu, C.; Chowdhury, S.; Lee, M. C.; Xiong, G.; Zhang, W.; Yang, R.; Cieplak, P.; Luo, R.; Lee, T.; Caldwell, J.; Wang, J.; Kollman, P. *J. Comput. Chem.* **2003**, *24*, 1999−2012.
(64) Hornak, V.; Abel, R.; Okur, A.; Strockbine, B.; Roitberg, A.; Simmerling, C. *Proteins* **2006**, *65*, 712−725.
(65) Lindorff-Larsen, K.; Piana, S.; Palmo, K.; Maragakis, P.; Klepis, J. L.; Dror, R. O.; Shaw, D. E. *Proteins* **2010**, *78*, 1950−1958.
(66) Lyubartsev, A. L. *Eur. Biophys. J.* **2005**, *35*, 53−61.
(67) Pan, J.; Heberle, F. A.; Tristam-Nagle, S.; Szymanski, M.; Koepfinger, M.; Katsaras, J.; Kučerka, N. *Biochim. Biophys. Acta* **2012**, *1818*, 2135−2148.
(68) Petrache, H. I.; Tristam-Nagle, S.; Gawrisch, K.; Harries, D.; Parsegian, V. A.; Nagle, J. F. *Biophys. J.* **2004**, *86*, 1574−1586.
(69) Chiu, S. W.; Vasudevan, S.; Jakobsson, E.; Mashi, R. J.; Scott, H. L. *Biophys. J.* **2003**, *85*, 3624−3635.
(70) Becke, A. D. *J. Chem. Phys.* **1993**, *98*, 5648−5652.
(71) Lee, C.; Wang, W.; Parr, R. G. *Phys. Rev. B* **1988**, *37*, 785−789.
(72) Vosko, S. H.; Wilk, L.; Nusair, M. *Can. J. Phys.* **1980**, *58*, 1200−1211.
(73) Stephens, P. J.; Devlin, F. J.; Chabalowski, C. F.; Frisch, M. J. *J. Phys. Chem.* **1994**, *98*, 11623−11627.
(74) Kendall, R. A.; Dunning, T. H.; Harrison, R. J. *J. Chem. Phys.* **1992**, *96*, 6796−6806.
(75) Bayly, C. I.; Cieplak, P.; Cornell, W.; Kollman, P. A. *J. Phys. Chem.* **1993**, *97*, 10269−10280.
(76) Tomasi, J.; Mennucci, B.; Cancés. *J. Mol. Struct.: THEOCHEM* **1999**, *464*, 211−226.
(77) Pomelli, C. S.; Tomasi, J.; Barone, V. *Theor. Chem. Acc.* **2001**, *105*, 446−451.
(78) Frisch, M. J.; et al. *Gaussian09*, Revision A.02; Gaussian Inc., Wallingford CT, 2009.
(79) Dupradeau, F. Y.; Pigache, A.; Zaffran, T.; Savineau, C.; Lelong, R.; Grivel, N.; Lelong, D.; Rosanski, W.; Cieplak, P. *Phys. Chem. Chem. Phys.* **2010**, *12*, 7821−7839.
(80) Hess, H.; Bekker, B.; Berendsen, H. J. C.; Fraaije, J. G. E. M. *J. Comput. Chem.* **1997**, *18*, 1463−1472.
(81) Miyamoto, S.; Kollman, P. A. *J. Comput. Chem.* **1992**, *13*, 952−962.
(82) Nosé, S. *J. Chem. Phys.* **1984**, *81*, 511−519.
(83) Hoover, W. G. *Phys. Rev. A* **1985**, *31*, 1695−1697.
(84) Parrinello, M.; Rahman, A. *J. Appl. Phys.* **1981**, *52*, 7182−7190.
(85) Darden, T.; York, D.; Pedersen, L. *J. Chem. Phys.* **1993**, *98*, 10089−10092.
(86) Essmann, U.; Perera, L.; Berkowitz, T.; Pedersen, L. G. *J. Chem. Phys.* **1995**, *103*, 8577−8593.
(87) Allen, M. P.; Tildesley, D. J. *Computer Simlations of Liquids*; Oxford University Press: Oxford, U. K., 1984; pp 64−65.
(88) Wong-ekkabut, J.; Karttunen, M. *J. Chem. Theory Comput.* **2012**, *8*, 2905−2911.
(89) Wong-ekkabut, J.; Miettinen, M. S.; Dias, C.; Karttunen, M. *Nat. Nanotechnol.* **2010**, *5*, 555−557.
(90) Åqvist, J. *J. Phys. Chem.* **1990**, *94*, 8021−8024.
(91) Jorgensen, W. L.; Chandrasekhar, J.; Madura, J. D.; Impey, R. W.; Klein, M. L. *J. Chem. Phys.* **1983**, *79*, 926−935.
(92) Hess, B.; Kutzner, C.; van der Spoel, D.; Lindahl, E. *J. Chem. Theory Comput.* **2008**, *4*, 435−447.
(93) Lyubartsev, A. P.; Laaksonen, A. *Comput. Phys. Commun.* **2000**, 565−589.
(94) Humphrey, W.; Dalke, A.; Schulten, K. *J. Mol. Graphics* **1996**, *14*, 33−38.
(95) Roux, B.; Karplus, M. *J. Phys. Chem.* **1991**, *95*, 4856−4868.
(96) Kubo, R. *Rev. Mod. Phys.* **1966**, *29*, 255−284.
(97) Marrink, S. J.; Berendsen, H. J. C. *J. Phys. Chem.* **1994**, *98*, 4155−4168.
(98) Braun, A. R.; Brandt, O.; Edholm, E. G.; Nagle, J. F.; Sachs, J. N. *Biophys. J.* **2011**, *100*, 2112−2120.

(99) Gurtovenko, A. A.; Miettinen, M.; Karttunen, M.; Vattulainen, I. *J. Phys. Chem. B* **2005**, *109*, 21126−21134.
(100) Miettinen, A. A.; Gurtovenko, M. S.; Vattulainen, I.; Karttunen, M. *J. Phys. Chem. B* **2009**, *113*, 9226−9234.
(101) Cordomí, A.; Edholm, O.; Perez, J. J. *J. Phys. Chem. B* **2008**, *112*, 1397−1408.
(102) Gurtovenko, A. A.; Vattulainen, I. *Biophys. J.* **2007**, *92*, 1878−1890.
(103) Cordomí, A.; Edholm, O.; Perez, J. J. *J. Chem. Theory Comput.* **2009**, *5*, 2125−2134.
(104) Maulik, P. R.; Sripada, P. K.; Shipley, G. G. *Biochim. Biophys. Acta* **1991**, *1062*, 211−219.
(105) Metcalf, R.; Pandit, S. A. *J. Phys. Chem. B* **2012**, *116*, 4500−4509.
(106) Niemelä, P. S.; Hyvönen, M. T.; Vattulainen, I. *Biophys. J.* **2006**, *90*, 851−863.
(107) Niemelä, P.; Hyvönen, M. T.; Vattulainen, I. *Biophys. J.* **2004**, *87*, 2976−2989.
(108) Anézo, C.; de Vries, A. H.; Höltje, H. D.; Tieleman, D. P.; Marrink, S. J. *J. Phys. Chem. B* **2003**, *107*, 9424−9433.
(109) Chiu, S.-W.; Pandit, S. A.; Scott, H. L.; Jakobsson, E. *J. Phys. Chem. B.* **2009**, *113*, 2748−2763.
(110) Kučerka, N.; Nagle, J. F.; Sachs, J. N.; Feller, S. E.; Pencer, J.; Jackson, A.; Katsaras, J. *Biophys. J.* **2008**, *95*, 2356−2367.
(111) Kučerka, N.; Holland, B. W.; Gray, C. G.; Tomberli, B.; Katsaras, J. *J. Phys. Chem. B* **2012**, *116*, 321−239.
(112) Maulik, P. R.; Shipley, G. G. *Biochemistry* **1996**, *34*, 8025−8034.
(113) Bartels, T.; Lankalapalli, R. S.; Bittman, R.; Beyer, K.; Brown, M. F. *J. Am. Chem. Soc.* **2008**, *130*, 14521−14532.
(114) Klauda, J. B.; Kučerka, N.; Brooks, B. R.; Pastor, R. W.; Nagle, J. F. *Biophys. J.* **2006**, *90*, 2796−2807.
(115) Kučerka, N.; Nieh, M.-P.; Katsaras, J. *Biochim. Biophys. Acta* **2011**, *1808*, 2761−2771.
(116) Vermeer, L. S.; de Groot, B. L.; Reat, V.; Milon, A.; Czaplicki, J. *Eur. Biophys. J.* **2007**, *36*, 919−931.
(117) Pandit, S. A.; Chiu, S. W.; Jakobsson, E.; Grama, A.; Scott, H. L. *Langmuir* **2008**, *24*, 6858−6865.
(118) Martinez-Seara, H.; Róg, T.; Pasenkiewicz-Gierulab, M.; Vattulainen, I.; Karttunen, M.; Reigada, R. *Biophys. J.* **2008**, *95*, 3295−3305.
(119) Trouard, T. P.; Nevzorov, A. A.; Alam, T. M.; Job, C.; Zajicek, J.; Brown, M. F. *J. Chem. Phys.* **1999**, *110*, 8802−8818.
(120) Rawicz, W.; Smith, B. A.; McIntosh, T. J.; Simon, S. A.; Evans, E. *Biophys. J.* **2008**, *94*, 4725−4736.
(121) Khelashvili, G.; Pabst, G.; Harries, D. *J. Phys. Chem. B* **2010**, *114*, 7524−7534.
(122) Hodzic, A.; Rappolt, M.; Amenitsch, H.; Laggner, P.; Pabst, G. *Biophys. J.* **2008**, *94*, 3935−3944.
(123) Mathai, J. C.; Tristam-Nagle, S.; Nagle, J. F.; Zeidel, M. L. *J. Gen. Physiol.* **2008**, *131*, 69−76.
(124) Aittoniemi, J.; Niemelä, P. S.; Hyvönen, M. T.; Karttunen, M.; Vattulainen, I. *Biophys. J.* **2007**, *92*, 1125−1137.
(125) van der Spoel, D.; van Maaren, P. J.; Berendsen, H. J. C. *J. Chem. Phys.* **1998**, *108*, 10220−10230.
(126) Mark, P.; Nilsson, L. *J. Phys. Chem. A* **2001**, *105*, 9954−9960.